applied optics

Time delay compensation method for tip–tilt control in adaptive optics system

Chongchong Wang,[1,2] Lifa Hu,[1,*] Yukun Wang,[1] Shaoxin Wang,[1] Quanquan Mu,[1] Dayu Li,[1] Zhaoliang Cao,[1] Chengliang Yang,[1] Huanyu Xu,[1] and Li Xuan[1]

[1]State Key Laboratory of Applied Optics, Changchun Institute of Optics, Fine Mechanics and Physics, Chinese Academy of Sciences, Changchun, Jilin 130033, China
[2]Chinese Academy of Sciences University, Beijing 100039, China
*Corresponding author: hulifa@ciomp.ac.cn

Received 19 November 2014; revised 5 March 2015; accepted 13 March 2015; posted 13 March 2015 (Doc. ID 225224); published 9 April 2015

The time delay engendered by wavefront sampling and data processing inevitability exists in almost all the wavefront sensor (WFS) based adaptive optics (AO) systems. Also, when WFS is used for tip–tilt aberration detection, the time delay significantly reduces the tip–tilt correction performance of the AO system. In this paper, we focus on researching time delay in a tip–tilt (TT) control system and introduce a predicted signal compensation method (PSCM) to compensate the time delay by modifying the WFS detected signals. Based on a precise model of a TT dynamic control system, the detection delay of TT corrections included in a WFS detected signal can be compensated. Experiments are conducted in the lab: the pure integrator (I), proportional and integral (PI) wavefront TT controllers, and these controllers with PSCM are compared to test the efficiency of the PSCM for TT corrections. For the PI controller, the rejection bandwidth increases from 52 to 62 Hz by using PCSM; meanwhile, the open-loop phase margin increases from 45 to 60 deg. In addition, astronomical observation results are also given based on the PI wavefront TT controller. The PSCM improves the Strehl ratio by a factor of 1.3. The new method is proven to improve the AO system closed-loop performance not only for increasing the closed-loop rejection bandwidth but also in favor of the error attenuation at low frequency. Furthermore, the method does not introduce more noise to the system. © 2015 Optical Society of America

OCIS codes: (010.1080) Active or adaptive optics; (010.1285) Atmospheric correction.

http://dx.doi.org/10.1364/AO.54.003383

1. INTRODUCTION

Adaptive optics (AO) is a technique that measures and compensates wavefront aberrations induced by the Earth's atmosphere and imperfections in the telescope optics to obtain the diffraction-limited image. In most AO systems, the wavefront correction is divided into two stages: a tip–tilt mirror (TTM) for correcting the tip–tilt (TT) aberrations and a deformable mirror (DM) for correcting the high-order aberrations [1,2]. Unlike adaptive optics based on the deformable mirror, our group uses the liquid-crystal spatial light modulator as the wavefront corrector for high-order aberration correction [3–7], while the TTM is also used to compensate TT disturbances based on the closed-loop control. Generally, the Shack–Hartman wavefront sensor (SHWFS) and an individual camera are used to detect the high-order and TT aberrations, respectively. Therefore, part of the incident light has to be used for TT detection, which decreases the light energy incident on SHWFS. But, in our liquid crystal adaptive optics system (LCAOS), in order to improve the optical energy utilization efficiency, a single sensor detection method is adopted; that is, only the SHWFS is used for both TT and high-order aberration sensing. When light spots are in the normal range of SHWFS subwindows, the average X and Y direction displacements of SHWFS are used to compute the TT and high-order aberration signals; when light spots are out of the normal range of SHWFS subwindows, the X and Y direction displacements of SHWFS light spots as a whole are used as the TT signals.

Because of the sampling and readout time of SHWFS, most SHWFS-based AO control systems have several sample period time delays, and, when using a conventional simple integrator (I) or proportional and integral (PI) controllers, this time delay significantly deteriorates the system performance. A direct way to solve this problem is to upgrade hardware and data processing methods. Hardware updating is difficult and laborious. Therefore, it is more effective to introduce a control strategy or a data processing method based on available adaptive optics system. A predictive control based on the dynamic characteristics of the atmospheric turbulence is an effective method to compensate the time delay. Wallner attempted to

reconstruct an estimate of the wavefront from the measured wavefront slope data [8]. Zuev and Lukin investigated the dynamic characteristics of the optical adaptive system and proposed the conception of predicting adaptive systems [9,10]. Since Schwartz *et al.* proposed that atmospheric turbulence measured by SHWFS was predictable in 1994 [11], many researchers have been investigating the prediction of the wavefront using different methods. P. McGuire *et al.* concentrated on the linear prediction of the wavefront slope in the open-loop system [12]. Jorgenson, Aitken, and Montera *et al.* used artificial neural networks to predict a turbulence wavefront slope [13,14]. For the linear slope prediction, the relatively larger computational complexity is difficult to overcome, and, for the artificial neural networks, it is easily plagued when running into local minima in the training error surface [12]. In recent years, a new kind of method based on a Kalman filter is widely used for atmospheric turbulence prediction [15,16]. However, no matter which predictor is used—adaptive linear predictor, predictor based on the artificial neural networks, or Kalman filter—all of them estimate the turbulence at a current sampling period or in several future sampling periods, according to several latest frames of aberrations. Thus, when seeing a condition get worse, high signal-to-noise (SNR) of SHWFS cannot be guaranteed, and the detected data becomes severely contaminated by noise, which leads to instability of the AO control system. Unlike a traditional predictive control method, whose prediction is based on the measured external turbulence, we present a predicted signal compensation method (PSCM) that only focuses on compensating the system time delay for the TTM response.

There is an obvious difference between our method and the traditional prediction method, which is complicated. The PSCM is mainly based on the control system's characteristics, which are controllable and easy to identify. The principle of the PSCM is simple. According to the system working time sequence, the WFS detected error signal is comprised of the incoming turbulence variations and TTM corrections. Though, because of the system time delay, the incoming turbulence cannot be obtained at the current sample time, the control system dynamic response could be identified in advance, and TTM corrections can be computed according to it in real time. Thus, based on sufficient knowledge of the system working time sequence and precise model of the control system, a more precise error signal without the detection delay of TTM response can be estimated. Obviously, the PSCM does not compensate the detection time delay for the varying turbulences. But the experimental results have shown that, by using the PSCM, the new adaptive optics system obtains a higher error attenuation bandwidth whatever the TT controller is, PI or I. Meanwhile, after the time delay compensation, the open-loop phase margin has increased. This method is, thus, a simple and practical way to compensate the time delay. Therefore, this method can be used in many other closed-loop time delay control systems.

This paper is organized as follows: Section 2 analyzes the TTM control system working time sequence and presents the signal modified method. In Section 3, in order to obtain a more precise dynamic response model of the TTM control system, the hysteresis nonlinearity of TTM actuators was first compensated. Then, by solving a system identification problem, an accurate TT correction signal can be obtained. Section 4 tests the PSCM introduced here with the PI and I controller, and the experimental results are given. Section 5 concludes this paper.

2. SYSTEM WORK TIMING ANALYSIS

The scheme of our closed-loop TTM control system is shown in Fig. 1. The meaning of the symbols is straightforward: ϕ^{tur} is the wavefront TT turbulence, n is the WFS detection noise, ϕ^{cor} is the TTM correction, and ϕ^{res} is the residual TT aberration.

In an AO system, a higher sample rate led to better correction precision, so WFS usually ran in the frame transfer mode, which meant the exposing and data reading-out processes overlapped. For bright targets, when an appropriate SNR on WFS can be achieved, the exposure time was set to be as small as possible in order to obtain a higher sample rate, while for faint targets the exposure time must be increased to obtain a reasonable SNR on WFS. Figure 2 illustrates the working time sequence of the common sampling and correction process. The top of this figure is the time axis, and T_s is the sampling period. Periods t1, t2, t3, and t4 represent the WFS exposure, the CCD readout, the data processing and voltage application, and the TTM response process, respectively. Among them, t1 and t2 could be set by the program, while their minimum value was constrained by hardware. Under this working operation, the time t4 for TTM response equaled to the exposure time t1.

Considering the k sampling period, light was integrated from $t \in [(k-1)T_s, kT_s]$, which is the t1 period shown in Fig. 2. From $t = kT_s$ onward, the CCD readout was denoted as the t2 period. The t3 period followed, which included wavefront slope data processing, control voltage computation, and TTM driving. At the end of data processing, the residual TT aberration signal $\phi^{\mathrm{res}}_{k+1}$ could be obtained. Meanwhile, control voltage $u(k+1)$ was applied and held by a zero-order holder for the next sampling period. Thus, $\phi^{\mathrm{res}}_{k+1}$ detected by WFS $t = (k+1)T_s$ was given by

$$\phi^{\mathrm{res}}_{k+1} = \frac{1}{T_s}\int_{(k-1)T_s}^{kT_s} [\phi^{\mathrm{tur}}(t) - \phi^{\mathrm{cor}}(t)]\mathrm{d}t. \tag{1}$$

Here, the detection noise was ignored for simplicity. The discrete-time form of Eq. (1) was

$$\phi^{\mathrm{res}}_{k+1} = \phi^{\mathrm{tur}}_{k} - \phi^{\mathrm{cor}}_{k}, \tag{2}$$

where ϕ^{cor}_{k} was the TTM correction corresponding to $u(k-1)$. From a system model perspective, the relationship between ϕ^{cor}_{k} and $u(k-1)$ could be described as an open-loop dynamic model of the TTM and WFS systems.

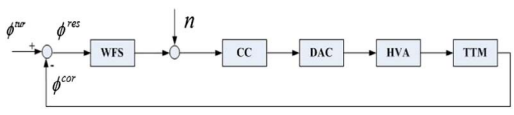

Fig. 1. TTM closed-loop control scheme. Here, CC represents the TT wavefront controller, while DAC and HVA represent the digital to analogue converter and high voltage amplifier, respectively.

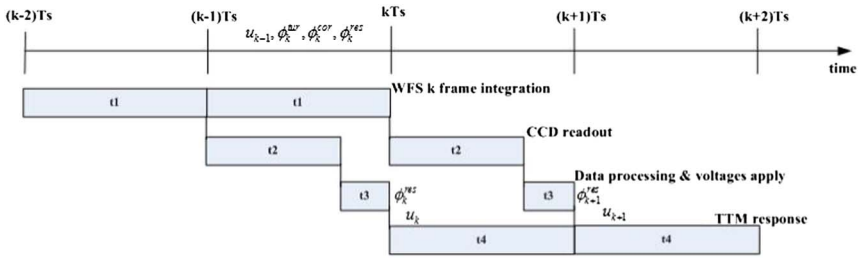

Fig. 2. Simplified temporal diagram of operations in TTM control system.

Obviously, ϕ_{k+1}^{res} was measured with one sampling period delay for external turbulences and TTM corrections, which had significantly deteriorated the control system's stability and performance. As for the external TT turbulences, though TT could not be measured in advance and its prediction was complicated, its variation during one sampling period was very small. Suppose that the TT turbulences varied along a sinusoid with the frequency of 20 Hz and the amplitude of one wavelength (λ). If the AO system sample rate was 1 kHz (the sample rate in our AO system was larger than 1 kHz), then the largest TT variation ($(\Delta\phi^{\text{tur}})_{\max}$) during one sample was 0.0022λ, according to the equation $(\Delta\phi^{\text{tur}})_{\max} = \sin(2\pi f * T_s)$. This variation could be ignored compared with signal ϕ^{res} (generally larger than 0.01λ for one unit wavelength).

On the other hand, the dynamic model of TTM control system could be identified in advance, and TTM corrections could be calculated earlier. Thus, a more precise residual aberration signal $\tilde{\phi}_{k+1}^{\text{res}}$ is in a modified version of Eq. (2) such that

$$\tilde{\phi}_{k+1}^{\text{res}} = \phi_k^{\text{tur}} - \phi_{k+1}^{\text{cor}}. \quad (3)$$

By doing this signal modifying process, the time delay compensation for TTM response was compensated. Thus, we called this time compensation method PSCM.

Then, the critical work was to find the system model, which was needed to calculate the ϕ^{cor} corresponding to the input voltage sequence $\{u(k)\}$. This was called system model identification in the control point of view.

3. HYSTERESIS NONLINEARITY COMPENSATION AND SYSTEM MODEL IDENTIFICATION

Generally, TTM was considered a linear second-order low-pass filter in the AO control system. However, the TTM actuated by piezo-ceramic actuators had inherent hysteresis nonlinearity, and this hysteresis made the linearity filter model precision low. Such an inaccurate TTM model cannot be used for the system response estimation. The hysteresis compensation (HC) for TTM was necessary before system model identification and delay compensation.

The piezo-ceramic actuator's hysteresis was proportional to the applied signal's frequency: the higher its frequency, the larger the TTM's hysteresis, which made HC a more challenging job. But, when the exciting frequency was so low that TTM could fully respond, the TTM would behave nearly the same as the static hysteresis response property, which did not change. Fortunately, the hysteresis nonlinearity of TTM used in our AO system usually worked close to this condition because the spectrum of external TT disturbance signals in AO system was mostly in a very low frequency (below 20 Hz) domain according to Tyler theory [17]. Therefore, the difference of TTM hysteresis nonlinearity for different low frequencies could be neglected during the correction process. The hysteresis curves under different exciting frequencies were measured, as shown in Fig. 3, which identified this hypothesis.

The feed-forward linearization with an inverse hysteresis model is proven to be a cost-effective approach for HC in AO systems [18,19]. It only required a mathematical model instead of hardware modification but, meanwhile, provided efficient correction on hysteresis. Thus, in this paper, the Presiach inverse hysteresis model was considered. Since there have been intensive investigations on the Presiach inverse hysteresis model, as mentioned previously and in our former publication [20], only the compensation results are presented briefly here. Figure 4 shows the hysteresis curves between the control voltage u and the measurement TTM displacement y when HC was off and on. In order to quantify the hysteresis nonlinearity of TTM, here define h_s as the ratio of the maximum possible output difference for any input ($\Delta y_{\max}$) divided by the output range (y_m), i.e., $h_s = \Delta y_{\max}/y_m$. The hysteresis parameter h_s had been reduced from 15.6% to 1.4% by HC, as shown in Fig. 5, and the linearity of the input–output curve had been significantly improved. Furthermore, the computation time of this method was on the order of 5–10 μs based on the hardware configuration in our lab, which could be ignored.

After HC, the transfer from the control voltage input u to the WFS detected output y became linear, and a linear dynamic

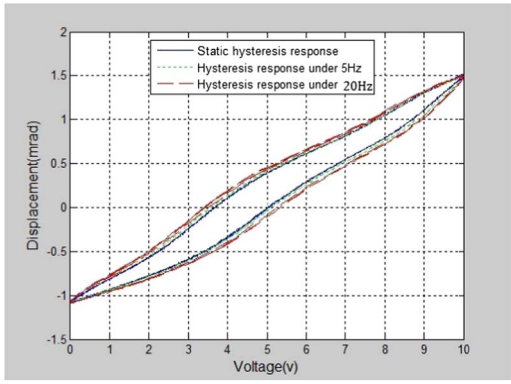

Fig. 3. TTM hysteresis curves under different exciting frequencies.

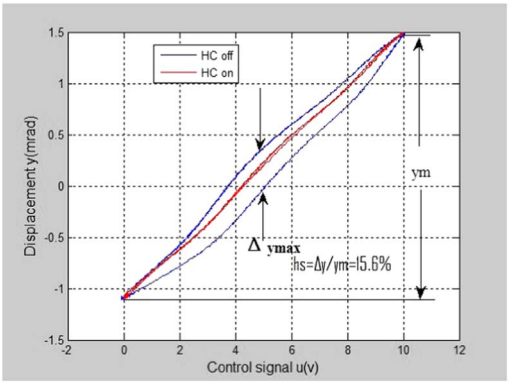

Fig. 4. Hysteresis curves with HC on and off.

model was identified for the controller design. The system model identification mainly included two steps: (1) determining model structure; (2) evaluating model parameters. Based on the system analysis above, we considered the system model as a two-order linear model with one sample time lag. Here, a subspace model identification method was used for the system model parameter identification.

4. EXPERIMENT AND RESULTS

A. Lab Experiment Setup

To validate the proposed strategy for TTM control, an experiment was conducted in the lab. Figure 5 shows a schematic of the experimental setup.

The object light collimated by lens L1 was reflected by a tip–tilt mirror (TTM1). Then, it passed through lens L2 and L3, and the wavefront TT aberrations were compensated by another tip–tilt mirror (TTM2). Finally, the corrected light was directed to WFS via lens L4 and L5. The TTM1, TTM2 surface, and the aperture of the WFS were conjugated with each other. In this experimental system, the two tip–tilt mirrors were all actuated by the PI high-dynamics piezo tip–tilt platform. TTM1 (PI S330) was introduced here to produce the incoming TT disturbances, while TTM2 (PI S334) was used as the TT aberration corrector with a resonance frequency of 1.7 kHz. By introducing TTM1, here we can measure the closed-loop frequency response and turbulence attenuation

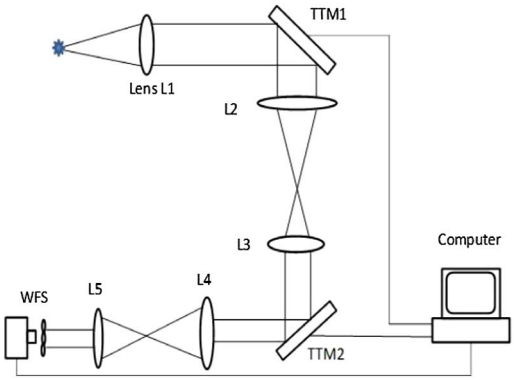

Fig. 5. Optical layout of the experimental TTM control system setup.

frequency response of the TT control system with different control strategies. Based on these, we can evaluate the system performance and optimize TT controllers. WFS made by our group was based on an OCAM2 camera. In the system frequency response measurement experiment, the sample rate was set to be the fastest 1.67 kHz, while the readout time t2 was 0.37 milliseconds (ms), which corresponded to the fastest CCD readout speed. Based on the current hardware configuration and software computation algorithm, wavefront data processing and control voltage computation time t3 was tested to be about 0.05 ms.

B. System Model Identification and Frequency Response Measurement Results in Lab

As illustrated in Section 2, the efficiency of PSCM depended on system model precision; thus, the precision of an identified system model was tested. First, excite the system in open loop with control input denoted as $u(k)$ and record the WFS measurement as $y(k)$. Then, by comparing the experimental output $y(k)$ with the estimation $\hat{y}(k)$ calculating from the system model, the accuracy of the system model was evaluated.

For the model identification, the $u(k)$ selection was critical and had much influence on the model precision. In general, white noise was usually used as the input signal. But, to our system, the actual TT disturbance induced by atmospheric turbulence had much difference with the white noise. Fortunately, the real-time voltage data applied for TT correction could be collected from the AO system at the 1.23 m telescope. Using this on-sky data helped to validate the TT control system dynamic model. Figure 6(a) shows a 2 s portion of one axis test data to illustrate the correlation of the model high-frequency dynamic response to that of the actual system empirical data. The model estimation errors are shown in Fig. 6(b), and the maximum estimation for this particular data set was 23 milli arc second (mas), and the standard deviation of the error signal amplitude between model and experimental data was 4 mas, which indicated the high precision of our model.

Then low-frequency (from 1 to 320 Hz) response tests were compared among the traditional I and PI controllers and these controllers with PSCM proposed in this paper. For a system under the constraint of a 45 deg phase margin (PM) and gain margin (GM) large than 6 dB, the closed-loop rejection transfer functions were plotted in Fig. 7.

When only the traditional I controller was used, the −3 dB disturbance rejection bandwidth, which was specified as the −3 dB magnitude cut-off frequency, was only 43 Hz. When PSCM was used with the I controller, it was improved to 56 Hz, while for the PI controller when using PSCM, the rejection bandwidth increased from 52 to 62 Hz. Meanwhile, the open-loop PM was increased from 45 to 60 deg with GM of little change. These results indicated that, with PSCM, the time delay for TTM response detection was compensated, which led the system −3 dB rejection bandwidth to increase by at least 10 Hz and improve the system stability as well.

The closed-loop static position error was also tested in the lab to research the noise amplification property of different control strategies. The same object light was used for different kinds of control strategy tests in order to guarantee that noise conditions remained unchanged. As shown in Fig. 8 for the

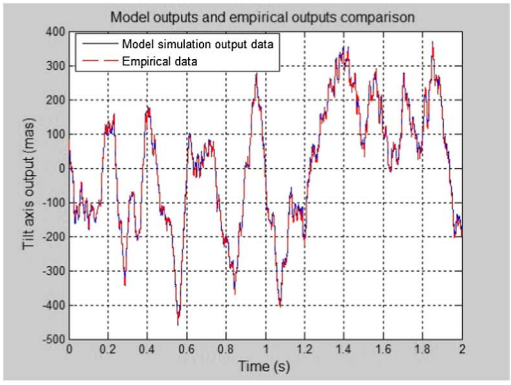

(a)

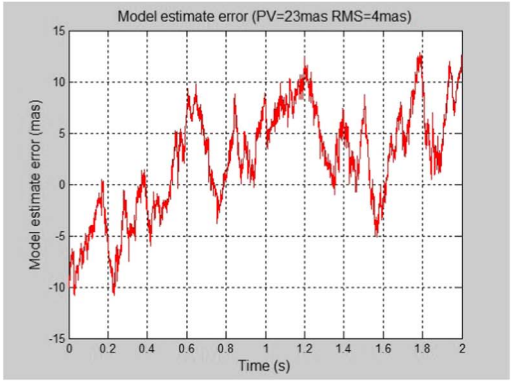

(b)

Fig. 6. Empirical system response data compared to the model data. (a) Empirical and model estimate output. (b) Estimation error.

same controller, the root mean square (rms) of the static position error were about the same no matter that the PSCM was used or not, which implied that the PSCM did not introduce more noise to the control system.

C. Observation Results on the 1.23 m Telescope

Adaptive correction experiments were also performed on a 1.23 m telescope with our adaptive optics system in our institution. Polaris with a visual magnitude of 2.44 was observed and corrected on November 9, 2014, with the Greenwood

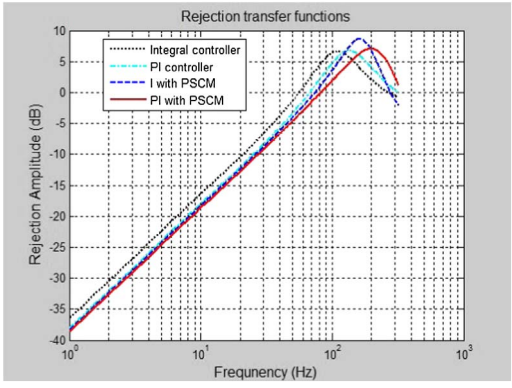

Fig. 7. Rejection transfer functions for I, PI controllers with and without PSCM.

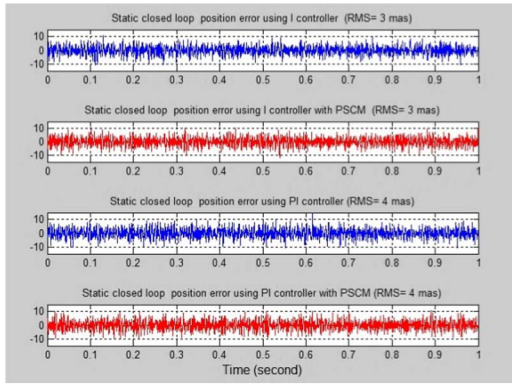

Fig. 8. Static position errors with different controllers. Maximum static position errors with PSCM and without PSCM were all about 20 mas.

frequency of about 70 Hz. To characterize the atmospheric turbulence, we used the SHWFS records continuous 1000 frames of light spots array pictures. The system sample rate was 1.67 kHz with the self-made WFS based on the

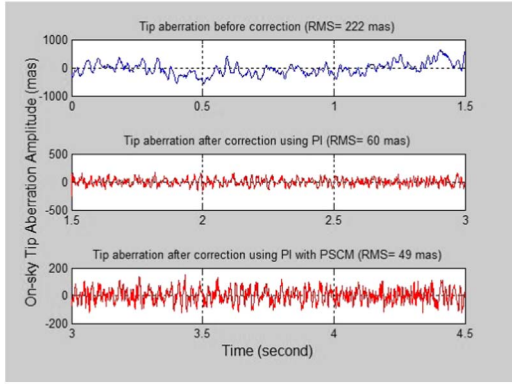

Fig. 9. 4.5 s portion of on-sky wavefront tip aberration data. (Before correction, the tip wavefront aberration was 222 mas rms. After correction with PI controller, it reduced to 60 mas rms; when PI was used with PSCM, it reduced further to 49 mas.)

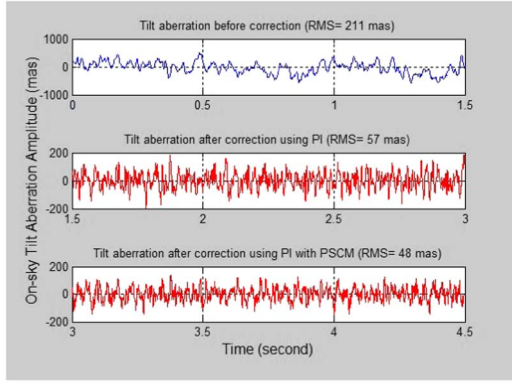

Fig. 10. 4.5 s portion of on-sky wavefront tilt aberration data. (Before correction, the tilt wavefront aberration rms was 211 mas. After correction with PI controller, it was reduced to 57 mas. When PI was used with PSCM, it was reduced further to 48 mas.)

OCAM2 camera. The Greenwood's frequency is calculated as 70 Hz. The data of tip–tilt aberrations for 4.5 s were collected in real-time during on-sky observation, as shown in Figs. 9 and 10. During first 1.5 s, the TT aberrations were not corrected, while at $t = 1.5$ s, the correction process began. The traditional PI controller was used from 1.5 to 3 s, then the control strategy transferred to PI controller with PSCM.

A large number of on-sky data showed that, when using a PI controller with PSCM, the rms of residual TT aberrations had been reduced by 16% on average compared with the PI controller only, which improved the Strehl ratio by a factor of at least 1.3.

5. CONCLUSIONS

The delay compensation strategy was introduced in this paper to improve the TTM closed-loop control system performance. Based on the dynamic characteristics of the TT corrector and detector, this control scheme predicts the system dynamic response behavior according to the excited voltages and positions in the past several sampling periods and further modifies the signal readout from the TT detector. Experimental results indicated that this optimized control for TT correction compensates the detection time delay for TTM response and improves the rejection −3 dB bandwidth of the TT control system as well as the system open-loop phase margin. Furthermore, the on-sky correction results showed that Strehl ratio had increased by at least 1.3 times on average, which illustrated the efficiency of the PSCM.

In fact, this method was helpful to most AO systems with time delay whether for TT or high-order aberration correction, especially for fainter target observation where the sample rate must decrease to achieve an appropriate SNR on the WFS detector, which resulted in a large time delay.

National Natural Science Foundation of China (NSFC) (11174274, 11204299, 61205021, 61377032, 61475152).

REFERENCES

1. D. T. Gavel, "Adaptive optics control strategies for extremely large telescopes," Proc. SPIE **4494**, 215–220 (2002).
2. C. Correia and J.-P. Véran, "Woofer–tweeter temporal correction split in atmospheric adaptive optics," Opt. Lett. **37**, 3132–3134 (2012).
3. Q. Mu, Z. Cao, L. Hu, D. Li, and L. Xuan, "An adaptive optics imaging system based on a high-resolution liquid crystal on silicon device," Opt. Express **14**, 8013–8018 (2006).
4. C. Li, M. Xia, Q. Mu, B. Jiang, L. Xuan, and Z. Cao, "High-precision open-loop adaptive optics system based on LC-SLM," Opt. Express **17**, 10774–10781 (2009).
5. Q. Mu, Z. Cao, L. Hu, Y. Liu, Z. Peng, L. Yao, and L. Xuan, "Open loop adaptive optics testbed on 2.16 meter telescope with liquid crystal corrector," Opt. Commun. **285**, 896–899 (2012).
6. C. Liu, L. Hu, Q. Mu, Z. Cao, and L. Xuan, "Open-loop control of liquid-crystal spatial light modulators for vertical atmospheric turbulence wavefront correction," Appl. Opt. **50**, 82–89 (2011).
7. L. Hu, L. Xuan, Y. Liu, Z. Cao, D. Li, and Q. Mu, "Phase-only liquid crystal spatial light modulator for wavefront correction with high precision," Opt. Express **12**, 6403–6409 (2004).
8. E. P. Wallner, "Optimal wave-front correction using slope measurements," J. Opt. Soc. Am. A **73**, 1771–1776 (1983).
9. V. E. Zuev and V. P. Lukin, "Dynamic characteristics of optical adaptive systems," Appl. Opt. **26**, 139–144 (1987).
10. V. P. Lukin, "Spectral and dynamic characteristics of the adaptive imaging system," Proc. SPIE **1688**, 453–464 (1992).
11. C. Schwartz, G. Baum, and E. Ribak, "Turbulence-degraded wave fronts as fractal surfaces," J. Opt. Soc. Am. A **11**, 444–451 (1994).
12. P. C. McGuire, T. A. Rhoadarmer, H. A. Coy, J. R. P. Angel, and M. Lloyd-Hart, "Linear zonal atmospheric prediction for adaptive optics," Proc. SPIE **4007**, 682–691, (2000).
13. M. B. Jorgenson and G. J. Aitken, "Prediction of atmospherically induced wave-front degradations," Opt. Lett. **17**, 466–468 (1992).
14. D. A. Montera, B. M. Welsh, M. C. Roggemann, and D. W. Ruck, "Prediction of wave-front sensor slope measurements with artificial neural networks," Appl. Opt. **36**, 675–681 (1997).
15. L. A. Poyneer and J.-P. Véran, "Kalman filtering to suppress spurious signals in adaptive optics control," J. Opt. Soc. Am. A **27**, A223–A234 (2010).
16. S. Meimon, C. Petit, T. Fusco, and C. Kulcsar, "Tip–tilt disturbance model identification for Kalman-based control scheme: application to XAO and ELT systems," J. Opt. Soc. Am. A **27**, A122–A132 (2010).
17. G. A. Tyler, "Bandwidth considerations for tracking through turbulence," J. Opt. Soc. Am. A **11**, 358–367 (1994).
18. Q. Yang, C. Ftaclas, M. Chun, and D. Toomey, "Hysteresis correction in the curvature adaptive optics system," J. Opt. Soc. Am. A **22**, 142–147 (2005).
19. A. Dubra, J. Massa, and C. Paterson, "Preisach classical and nonlinear modeling of hysteresis in piezoceramic deformable mirrors," Opt. Express **13**, 9062–9070 (2005).
20. C. Wang, B. He, L. Hu, Q. Mu, H. Song, and L. Xuan, "Hysteresis compensation method of piezoelectric steering mirror based on neural network," Chin. J. Lasers **40**, 239–244 (2013).